Available online at www.sciencedirect.com
ScienceDirect
Journal of Computational Physics 221 (2007) 41–62
JOURNAL OF COMPUTATIONAL PHYSICS
www.elsevier.com/locate/jcp

Nonreflecting boundary condition for time-dependent multiple scattering ☆

Marcus J. Grote [a,*], Christoph Kirsch [b]

[a] Department of Mathematics, University of Basel, Rheinsprung 21, CH-4051 Basel, Switzerland
[b] INRIA, Domaine de Voluceau – Rocquencourt, B.P. 105, F-78153 Le Chesnay Cedex, France

Received 13 December 2005; received in revised form 1 June 2006; accepted 2 June 2006
Available online 25 July 2006

Abstract

An exact nonreflecting boundary condition (NBC) is derived for the numerical solution of time-dependent multiple scattering problems in three space dimensions, where the scatterer consists of several disjoint components. Because each sub-scatterer can be enclosed by a separate artificial boundary, the computational effort is greatly reduced and becomes independent of the relative distances between the different sub-domains. In fact, the computational work due to the NBC only requires a fraction of the computational work inside Ω, due to any standard finite difference or finite element method, independently of the mesh size or the desired overall accuracy. Therefore, the overall numerical scheme retains the rate of convergence of the interior scheme without increasing the complexity of the total computational work. Moreover, the extra storage required depends only on the geometry and not on the final time. Numerical examples show that the NBC for multiple scattering is as accurate as the NBC for a single convex artificial boundary [M.J. Grote, J.B. Keller, Nonreflecting boundary conditions for time-dependent scattering, J. Comput. Phys. 127(1) (1996), 52–65], while being more efficient due to the reduced size of the computational domain.

MSC: 65M99; 74J05; 74J20; 76Q05; 78A40; 78A45

PACS: 43.20.Fn

Keywords: Time-dependent waves; Wave equation; Unbounded domain; Nonreflecting boundary condition; Artificial boundary condition; Multiple scattering

1. Introduction

When an incident wave encounters an obstacle, it is scattered in the unbounded surrounding medium. If two or more obstacles are present, the field scattered from one obstacle will induce further scattered fields from all the other obstacles, which again will induce further scattered fields from all obstacles, and so forth. Such

☆ This work is partially supported by the Swiss National Science Foundation.
* Corresponding author. Tel.: +41 61 267 39 96.
E-mail addresses: Marcus.Grote@unibas.ch (M.J. Grote), Christoph.Kirsch@inria.fr (C. Kirsch).

0021-9991/$ - see front matter © 2006 Elsevier Inc. All rights reserved.
doi:10.1016/j.jcp.2006.06.007

multiple scattering problems occur in a wide variety of applications from acoustics, electromagnetics, and elasticity [26]. Thus, we seek efficient numerical methods to compute the total scattered field for time-dependent multiple scattering problems.

A well-known approach for the numerical solution of scattering problems in unbounded regions is to enclose all obstacles, inhomogeneities, and nonlinearities with an artificial boundary B. A boundary condition is then imposed on B, which leads to a numerically solvable initial-boundary value problem in a bounded domain Ω. The boundary condition should be chosen such that the solution of the problem in Ω coincides with the restriction to Ω of the solution in the original unbounded region.

The numerical solution of the initial-boundary value problem in Ω contains two independent sources of error: the discretization error in the interior, due to the finite difference or finite element method used inside Ω, and the discretization error at the artificial boundary, due to some approximation used at B. To achieve convergence, both error components must be reduced systematically and simultaneously, as the mesh is refined, while the computational work due to the boundary condition at B should remain only a fraction of the computational work inside Ω, independently of the desired accuracy. Otherwise, the boundary condition imposed at B will be too expensive and impractical.

When the scatterer consists of several obstacles, which are well separated from each other, the use of a single artificial boundary to enclose the entire scattering region becomes too expensive. Instead it is preferable to enclose every sub-scatterer by a separate artificial boundary B_j. Then we seek an exact boundary condition on $B = \cup B_j$, where each B_j surrounds a single computational sub-domain Ω_j. This boundary condition must not only let outgoing waves leave Ω_j without spurious reflection from B_j, but also propagate the outgoing wave from Ω_j to all other sub-domains, which it may reenter subsequently. To derive such an exact boundary condition, an analytic representation of the solution everywhere in the exterior region is needed. Neither absorbing boundary conditions [3,8,31], nor perfectly matched layers [4,5,7] provide such an expression.

Thus far numerical methods for time-dependent multiple scattering have mainly been based on boundary integral formulations, where the exact boundary condition is usually obtained from a retarded potential boundary integral equation [19]. Similarly, an exact boundary condition was proposed by Ting and Miksis [30], and later implemented by Givoli and Cohen [10]. It is based on a Kirchhoff integral representation of the solution on B and requires storing the solution at a distinct surface strictly inside B for the length of time it takes to propagate across Ω. Recently, Teng [29] derived a modified version that only employs a single artificial boundary; it also eliminates the long-time numerical instability, which had previously been observed in [10].

Nevertheless, the straightforward evaluation of Kirchhoff-type boundary integrals for use as artificial boundary conditions is too expensive. If N_h denotes the typical number of grid points used in any space dimension, the number of grid points inside Ω scales like N_h^3 and that on the (two-dimensional) artificial boundary like N_h^2. Hence, the computational work *per time step* inside Ω, due to any typical finite difference or finite element method, scales like N_h^3. However, to update the solution at any particular point on the artificial boundary, a two-dimensional space–time integral is required over past values on B, so that any Kirchhoff-integral based boundary condition involves $O(N_h^4)$ operations per time step at B. As a consequence, the boundary condition is one order of magnitude more expensive than the numerical method used in the interior. Currently much research in boundary integral methods is devoted to reducing that computational cost [6,9,25].

To avoid the difficulties mentioned above, we shall seek a nonreflecting boundary condition (NBC) for multiple scattering, based on a superposition of Fourier series representations of the solution in the exterior region. Exact NBCs for time-dependent acoustic waves have been derived by Grote and Keller [12–14], Hagstrom and Warburton [22], or Sofronov [28], – see also [1,20] – but always in the situation of a single computational domain. In a situation of multiple disjoint domains, however, waves are not purely outgoing outside the computational domain $\Omega = \cup \Omega_j$, as they may bounce back and forth between domains. We shall show how to overcome this difficulty and derive an exact NBC for multiple scattering. Because this exact boundary condition allows the size of the computational sub-domains, Ω_j, to be chosen independently of the relative distances between them, the computational domain, Ω, can be chosen much smaller than that resulting from the use of a single convex computational domain.

In Section 2, we derive the exact nonreflecting boundary condition for two scatterers. By combining Fourier series representations with a progressive wave expansion by Wilcox [32], we show how to efficiently evaluate

the boundary operators involved. The solution of the initial-boundary value problem in Ω, with this NBC imposed on B, is shown to coincide with the restriction to Ω of the solution in the unbounded region Ω_∞. The formulation is generalized to an arbitrary number of scatterers in Section 3. In Section 4, we examine the computational cost of the multiple scattering NBC, and show that its complexity scales like N_h^3, too. We also discuss in detail an explicit finite difference implementation. In Section 5, we demonstrate the accuracy and convergence of the numerical scheme. We also compare the multiple scattering approach with the known NBC for a single spherical artificial boundary [13,14], and show that the numerical solutions obtained by these two different methods coincide. Finally, numerical experiments for an incident plane wave impinging on two sound-soft spheres illustrate the stability and high accuracy of the NBC.

2. Two scatterers

We consider acoustic wave scattering from two bounded disjoint scatterers in unbounded three-dimensional space. Each scatterer may contain one or several obstacles, inhomogeneities, and nonlinearity. We let Γ denote the piecewise smooth boundary of all obstacles and impose on Γ a Dirichlet-type boundary condition, for simplicity. In Ω_∞, the unbounded region outside Γ, the scattered field $U = U(\boldsymbol{x}, t)$ then solves the following initial-boundary value problem:

$$\frac{\partial^2 U}{\partial t^2} - \operatorname{div}(\underline{\boldsymbol{A}}\nabla U) = F \quad \text{in } \Omega_\infty \times I, \qquad I := (0,T), \quad T > 0, \tag{1}$$

$$U = U_0 \quad \text{in } \Omega_\infty \times \{0\}, \tag{2}$$

$$\frac{\partial U}{\partial t} = V_0 \quad \text{in } \Omega_\infty \times \{0\}, \tag{3}$$

$$U = G \quad \text{on } \Gamma \times I. \tag{4}$$

The material properties described by $\underline{\boldsymbol{A}}$ may vary in space, while both F and G can vary in space and time; F may also be nonlinear.

Next, we assume that both scatterers are *well separated*, that is we assume that we can surround them by two nonintersecting spheres B_1, B_2 centered at c_1, c_2 with radii R_1, R_2, respectively. In the unbounded region D, outside the two spheres, we assume that the medium is homogeneous and isotropic, that is $\underline{\boldsymbol{A}} \equiv c^2\underline{\boldsymbol{I}}$, where $c > 0$ constant and $\underline{\boldsymbol{I}}$ the identity. Moreover, we assume that the source F and the initial values U_0, V_0 vanish in $\overline{D}$. Thus, in the exterior region the scattered wave U satisfies the homogeneous wave equation with constant wave speed c and homogeneous initial conditions,

$$\frac{1}{c^2}\frac{\partial^2 U}{\partial t^2} - \Delta U = 0 \quad \text{in } D \times I, \qquad c > 0 \text{ constant}, \tag{5}$$

$$U = 0 \quad \text{in } D \times \{0\}, \tag{6}$$

$$\frac{\partial U}{\partial t} = 0 \quad \text{in } D \times \{0\}. \tag{7}$$

Because of the finite speed of propagation and the compact support of the initial data, the scattered field U is purely radiating at large distance.

We wish to compute the scattered wave, U, in the computational domain $\Omega = \Omega_\infty \backslash D$, which consists of the two disjoint components Ω_1 and Ω_2. Hence Ω is internally bounded by $\Gamma = \Gamma_1 \cup \Gamma_2$, and externally by $B = \partial D$, which consists of the two spheres B_1 and B_2 – see Fig. 1. To solve the scattering problem (1)–(4) inside Ω, a boundary condition is needed at the exterior *artificial boundary* $B = B_1 \cup B_2$. This boundary condition must ensure that the solution in Ω, with that boundary condition imposed on B, coincides with the restriction to Ω of the solution in the original unbounded region Ω_∞.

2.1. Nonreflecting boundary condition

In contrast to the situation of a single spherical artificial boundary, as considered for example by Hagstrom and Hariharan [21], Sofronov [28], or Grote and Keller [13], we cannot simply expand u outside B either in

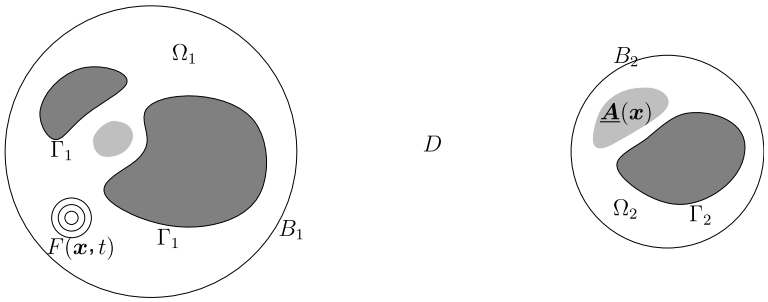

Fig. 1. A typical configuration with two scatterers is shown. Each scatterer consists of possibly several obstacles bounded by Γ_1 and Γ_2, but may also contain inhomogeneity, anisotropy, nonlinearity and sources. The computational domain $\Omega = \Omega_1 \cup \Omega_2$ is externally bounded by the artificial boundary $B = B_1 \cup B_2$; the unbounded region outside Ω is denoted by D.

Fourier series or as a superposition of purely outgoing multipole fields. In fact, since part of the scattered field leaving Ω_1 will reenter Ω_2 at later times, and vice versa, u is not outgoing in D. Thus, the boundary condition we seek at B must not only let outgoing waves leave Ω_1 without spurious reflection from B_1, but also propagate that wave field to Ω_2, and so forth, without introducing any spurious reflections.

The outgoing field, as seen from Ω_1, is fully determined by its boundary values on B_1, while the incoming field is fully determined by its boundary values on all other spheres. Because those values are time-retarded, they are already known, so that the entire scheme remains explicit in time. Moreover, because the initial conditions are confined to individual subdomains, the initial distribution of outgoing fields is known at $t = 0$ and can be tracked with increasing time.

Let D_1 denote the unbounded region outside B_1 and D_2 the unbounded region outside B_2. We now decompose the scattered wave U inside $D = D_1 \cap D_2$ in two purely outgoing waves U_1 and U_2, which solve the following two problems:

$$\frac{1}{c^2}\frac{\partial^2 U_1}{\partial t^2} - \Delta U_1 = 0 \quad \text{in } D_1 \times I, \tag{8}$$

$$U_1 = 0 \quad \text{in } D_1 \times \{0\}, \tag{9}$$

$$\frac{\partial U_1}{\partial t} = 0 \quad \text{in } D_1 \times \{0\} \tag{10}$$

and

$$\frac{1}{c^2}\frac{\partial^2 U_2}{\partial t^2} - \Delta U_2 = 0 \quad \text{in } D_2 \times I, \tag{11}$$

$$U_2 = 0 \quad \text{in } D_2 \times \{0\}, \tag{12}$$

$$\frac{\partial U_2}{\partial t} = 0 \quad \text{in } D_2 \times \{0\}. \tag{13}$$

We remark that (8)–(10) define an outgoing wave U_1, as seen from B_1, propagating with finite speed c into D_1, and similarly for (11)–(13) and U_2. In fact, each wave field is only influenced by a single scatterer and completely oblivious to the other. Therefore, U_1 and U_2 are entirely determined by their values on B_1 or B_2, respectively [24]. We now couple U_1 and U_2 with U by matching the values of $U_1 + U_2$ with those of U at $B = B_1 \cup B_2$:

$$U_1 + U_2 = U \quad \text{on } B \times I. \tag{14}$$

The two wave fields U and $U_1 + U_2$ both solve the homogeneous wave equation (5) in D, together with zero initial conditions (6) and (7). Since U and $U_1 + U_2$ coincide on B, they must coincide everywhere and for all time in the exterior region $\overline{D}$ (up to the boundary), because the initial-boundary value problem in $\overline{D}$ is well posed [24]. We summarize this result in the following proposition. Moreover, before proceeding with the derivation of the nonreflecting boundary condition, we shall also prove that the decomposition $U = U_1 + U_2$ introduced above always exists and is unique.

Proposition 1. *Let U solve the exterior Dirichlet problem (1)–(4) and assume that U satisfies (5)–(7) in the exterior region D. Then,*

$$U \equiv U_1 + U_2 \quad \text{in } \overline{D} \times I, \tag{15}$$

where U_1 and U_2 are solutions to the problems (8)–(10) and (11)–(13), respectively, together with the matching condition (14). The decomposition of U into the two purely outgoing waves U_1 and U_2 is unique.

Proof. By the argument above we have already shown that if $U = U_1 + U_2$ on $B \times I$, where U_1 and U_2 solve (8)–(13), then $U \equiv U_1 + U_2$ everywhere in $\overline{D} \times I$. We shall now show that U_1 and U_2 exist and, in fact, are unique.

Existence. In the exterior region $D \times I$ we use Kirchhoff's formula (see, for instance, [2]) to write

$$U(\boldsymbol{x},t) = \frac{1}{4\pi} \int_B \left\{ [U] \frac{\partial}{\partial \boldsymbol{n}} \left(\frac{1}{\rho}\right) - \frac{1}{c\rho} \frac{\partial \rho}{\partial \boldsymbol{n}} \left[\frac{\partial U}{\partial t}\right] - \frac{1}{\rho} \left[\frac{\partial U}{\partial \boldsymbol{n}}\right] \right\} \mathrm{d}s, \tag{16}$$

for $(\boldsymbol{x}, t) \in D \times I$. Here, and everywhere else throughout this paper $[f] := f(t - \rho/c)$ denotes the retarded values of any time-dependent function f, while $\rho := |\boldsymbol{x} - \boldsymbol{y}|$, $\boldsymbol{y} \in B$, and $\boldsymbol{n}$ denotes the unit normal vector pointing into D. Let

$$U_j(\boldsymbol{x},t) = \frac{1}{4\pi} \int_{B_j} \left\{ [U] \frac{\partial}{\partial \boldsymbol{n}} \left(\frac{1}{\rho}\right) - \frac{1}{c\rho} \frac{\partial \rho}{\partial \boldsymbol{n}} \left[\frac{\partial U}{\partial t}\right] - \frac{1}{\rho} \left[\frac{\partial U}{\partial \boldsymbol{n}}\right] \right\} \mathrm{d}s, \tag{17}$$

$(\boldsymbol{x}, t) \in D_j \times I$, $j = 1, 2$. Because (17) is a combination of single and double layer retarded potentials with densities $U|_{B_j}$, $\partial_t U|_{B_j}$, $\partial_n U|_{B_j}$, the functions U_j each solve the wave equation in $D_j \times I$, $j = 1, 2$ [2]. Clearly, $U_1(\boldsymbol{x}, t) + U_2(\boldsymbol{x}, t) = U(\boldsymbol{x}, t)$, everywhere in $D \times I$. With the jump relations for retarded potentials, the expressions (16) and (17) can be extended up to the artificial boundaries B and B_1, B_2, respectively. Thus, U_1 and U_2 also satisfy the matching condition (14).

Uniqueness. Let $U = V_1 + V_2$ be another decomposition in $\overline{D} \times I$, where V_1 and V_2 solve (8)–(10) and (11)–(13), respectively. We shall now show that $V_1 \equiv U_1$ and that $V_2 \equiv U_2$ in $\overline{D} \times I$. To do so, we let $W_1 := U_1 - V_1$ and $W_2 := U_2 - V_2$. Hence, W_1 and W_2 satisfy (8)–(10) and (11)–(13), respectively, while their sum $W_1 + W_2 = U_1 + U_2 - (V_1 + V_2) \equiv 0$ in $\overline{D} \times I$.

Now, let $\delta > 0$ denote the distance between B_1 and B_2 and consider the two concentric open balls G_j B_j, $j = 1,2$, each at distance $\delta/2$ – see Fig. 2. Because each W_j is zero outside B_j at time $t = 0$, it remains zero outside G_j until the time $t_1 := \delta/(2c)$, due to the finite speed of propagation. In particular, W_1 vanishes inside G_2 for $t \leqslant t_1$. Therefore, $W_2 = -W_1$ must also vanish in $\overline{D}_2 \cap G_2$, and thus everywhere in D_2 up to time t_1. Similarly, we have $W_1 = 0$ in $D_1 \times [0, t_1]$.

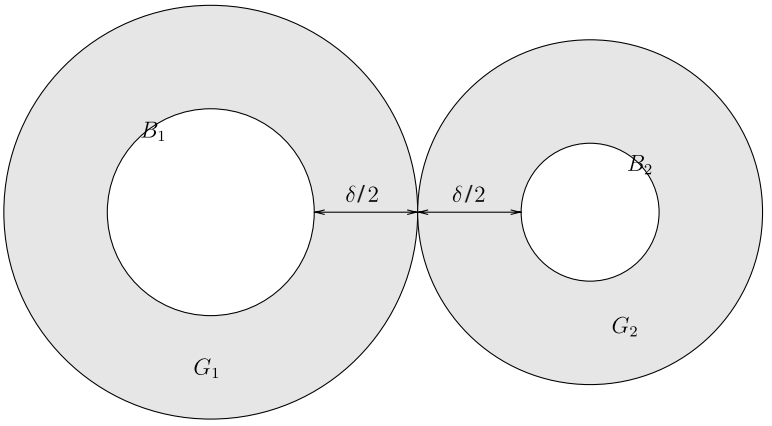

Fig. 2. The construction used in the proof of Proposition 1: the sphere B_j is contained in the concentric open ball G_j, $j = 1, 2$. The shortest distance between the two artificial boundary components is $\delta > 0$. The shaded regions correspond to $D_1 \cap G_1$ and $D_2 \cap G_2$, respectively.

Next, we consider the time interval $[t_1, t_2]$ with $t_2 := t_1 + \delta/(2c)$. Because each W_j is zero outside B_j at time $t = t_1$, it remains zero outside G_j up to time t_2. From the argument above, we conclude that $W_j \equiv 0$ in $D_j \times [0, t_2]$. The same argument may be used repeatedly until the final time T is reached. □

As a consequence of Proposition 1, the decomposition of U in two outgoing wave fields U_1, U_2 is well defined and we may now use it to determine a nonreflecting boundary condition for U on B. At B_1, for instance, the wave field U at any instant consists of both an outgoing wave U_1 and an incoming wave U_2. Since U_1 is purely outgoing as seen from Ω_1, it satisfies the exact nonreflecting boundary condition [13] at B_1, whereas the field U_2 at B_1 is fully determined by its previous values at B_2.

In $\overline{D}_j$, $j = 1, 2$, we now introduce the (local) spherical coordinates (r_j, ϕ_j, θ_j), where $r_j \geqslant R_j$ denotes the radial, $\phi_j \in [0, 2\pi)$ the longitudinal, and $\theta_j \in [0, \pi]$ the azimuthal variable, respectively. Then,

$$\mathscr{B}_1 U := \left(\frac{1}{c}\frac{\partial}{\partial t} + \frac{\partial}{\partial r_1}\right)(r_1 U) = M_1 U_1 + T_{12} U_2 \quad \text{on } B_1 \times I, \tag{18}$$

$$\mathscr{B}_2 U := \left(\frac{1}{c}\frac{\partial}{\partial t} + \frac{\partial}{\partial r_2}\right)(r_2 U) = M_2 U_2 + T_{21} U_1 \quad \text{on } B_2 \times I, \tag{19}$$

$$U_1 + P_{12} U_2 = U \quad \text{on } B_1 \times I, \tag{20}$$

$$P_{21} U_1 + U_2 = U \quad \text{on } B_2 \times I. \tag{21}$$

Here, the operator M corresponds to the (well known) exact nonreflecting boundary condition for a single computational domain [13,14]:

$$(\mathscr{B}_j U_j)(R_j, \phi_j, \theta_j, t) = (M_j U_j)(\phi_j, \theta_j, t), \quad j = 1, 2. \tag{22}$$

The *transfer operator*, T, and the *propagation operator*, P, are defined as

$$(T_{12} U_2)(\phi_1, \theta_1, t) := (\mathscr{B}_1 U_2)(R_1, \phi_1, \theta_1, t), \tag{23}$$

$$(T_{21} U_1)(\phi_2, \theta_2, t) := (\mathscr{B}_2 U_1)(R_2, \phi_2, \theta_2, t), \tag{24}$$

$$(P_{12} U_2)(\phi_1, \theta_1, t) := U_2(R_1, \phi_1, \theta_1, t), \tag{25}$$

$$(P_{21} U_1)(\phi_2, \theta_2, t) := U_1(R_2, \phi_2, \theta_2, t). \tag{26}$$

To utilize (22)–(26) in computation, we shall need explicit formulas to efficiently evaluate M, P, and T. In particular, we shall need the means to evaluate an outgoing wave and its partial derivatives anywhere in D, given its (past) values on B.

Clearly, the direct evaluation of M, P, or T via Kirchhoff type integrals, such as (16), is possible, yet it would require a two-dimensional space–time integral over B for *every* point on B. The resulting computational work would be one order of magnitude higher than that required in the interior, and thus too high a price to pay. Instead, we shall derive an analytic representation for U that holds everywhere in D and thus permits the efficient evaluation of all required quantities, without the need for space–time integration.

2.2. Wilcox expansion and efficient evaluation of M

By combining Fourier series with a progressive wave expansion by Wilcox, we shall now derive an analytic representation for any outgoing wave field U_j in terms of its values at B_j, which holds everywhere outside of B_j. Moreover, that expression will be more efficient than the direct evaluation via Kirchhoff's formula (16). Based on that representation formula, we shall then derive an explicit expression for M_j in (22), which incidentally coincides with the exact nonreflecting boundary condition proposed in [13,14].

Since the same expression will be used for every individual field U_j, we now omit the index of the corresponding subdomain for the rest of this section. Let $U = U(r, \phi, \theta, t)$ be a purely outgoing wave field, which satisfies the homogeneous wave equation with constant coefficients and zero initial conditions (5)–(7) in the region D, outside the sphere B of radius $R > 0$ centered at the origin. By calculating the inverse Laplace transform of the well-known expansion by Wilcox ([32], Eqs. (4) and (5)), we readily obtain the *progressive wave expansion*

$$U(r, \phi, \theta, t) = \frac{1}{r}\sum_{k=0}^{\infty} \frac{f^k(\phi, \theta, t - r/c)}{r^k}, \quad r > R, \tag{27}$$

which was also used by Bayliss and Turkel [3] and by Hagstrom and Hariharan [21]. Here the functions f^k, $k \geqslant 1$, are determined by f^0 via the recursion formula

$$\frac{1}{c}\frac{\partial f^k}{\partial t} = -\frac{\Delta_S + k(k-1)}{2k} f^{k-1}, \quad k \geqslant 1, \tag{28}$$

with $f^k(\phi, \theta, t) = 0$ for $t \leqslant 0$, while Δ_S denotes the Laplace–Beltrami operator on the unit sphere,

$$\Delta_S = \frac{1}{\sin\theta}\frac{\partial}{\partial\theta}\left(\sin\theta\frac{\partial}{\partial\theta}\right) + \frac{1}{\sin^2\theta}\frac{\partial^2}{\partial\phi^2}. \tag{29}$$

Let Y_{nm} denote the spherical harmonics normalized over the unit sphere, given by

$$Y_{nm}(\phi,\theta) = \sqrt{\frac{(2n+1)(n-|m|)!}{4\pi(n+|m|)!}} P_n^{|m|}(\cos\theta)\, e^{im\phi}, \quad 0 \leqslant |m| \leqslant n, \tag{30}$$

where $P_n^{|m|}$ denote the associated Legendre functions [23]. We now expand f^k in Fourier series, which yields

$$f^k(\phi,\theta,t) = \sum_{n=0}^{\infty}\sum_{m=-n}^{n} f_{nm}^k(t) Y_{nm}(\phi,\theta), \quad k \geqslant 0. \tag{31}$$

Because the spherical harmonics are eigenfunctions of Δ_S and satisfy

$$\Delta_S Y_{nm} = -n(n+1) Y_{nm}, \tag{32}$$

we obtain from (28) the recursion

$$\frac{1}{c}\frac{\mathrm{d}}{\mathrm{d}t} f_{nm}^k = \frac{(n+k)(n-k+1)}{2k} f_{nm}^{k-1}, \quad k \geqslant 1 \tag{33}$$

with $f_{nm}^k(t) = 0$ for $t \leqslant 0$, $k \geqslant 0$. From (33), we also observe that

$$f_{nm}^k \equiv 0, \quad k > n. \tag{34}$$

Next, we combine (27), (31), and (34) to obtain the Fourier series representation

$$U(r,\phi,\theta,t) = \sum_{n=0}^{\infty}\sum_{m=-n}^{n} U_{nm}(r,t) Y_{nm}(\phi,\theta), \quad r > R \tag{35}$$

with Fourier coefficients

$$U_{nm}(r,t) = \frac{1}{r}\sum_{k=0}^{n} \frac{f_{nm}^k(t-r/c)}{r^k}. \tag{36}$$

Hence, the wave field U is a superposition of infinitely many purely outgoing one-dimensional waves, f_{nm}^k. For $1 \leqslant k \leqslant n$, the functions f_{nm}^k are entirely determined by f_{nm}^0 through the recursion (33), whereas f_{nm}^0 is determined by the boundary values of U. Indeed, evaluating (36) at $r = R$ and solving for f_{nm}^0 yields

$$f_{nm}^0(t-R/c) = RU_{nm}(R,t) - \sum_{k=1}^{n} \frac{f_{nm}^k(t-R/c)}{R^k}. \tag{37}$$

Then, we introduce (37), with t replaced by $t-(r-R)/c$, into (36) and thus obtain

$$\begin{aligned} rU_{nm}(r,t) &= f_{nm}^0\left(t - \frac{r-R}{c} - \frac{R}{c}\right) + \sum_{k=1}^{n}\left(\frac{R}{r}\right)^k \frac{f_{nm}^k\left(t-\frac{r-R}{c}-\frac{R}{c}\right)}{R^k} \\ &\overset{(37)}{=} RU_{nm}\left(R, t-\frac{r-R}{c}\right) - \sum_{k=1}^{n}\frac{f_{nm}^k\left(t-\frac{r-R}{c}-\frac{R}{c}\right)}{R^k} + \sum_{k=1}^{n}\left(\frac{R}{r}\right)^k \frac{f_{nm}^k\left(t-\frac{r-R}{c}-\frac{R}{c}\right)}{R^k} \\ &= R[U_{nm}(R,\cdot)] - \sum_{k=1}^{n}\left(1-\left(\frac{R}{r}\right)^k\right)[\psi_{nm}^k]. \end{aligned} \tag{38}$$

Here $[f] := f(t-(r-R)/c)$ again denotes the retarded values of any function f; the functions ψ_{nm}^k are defined by

$$\psi_{nm}^k(t) := \frac{f_{nm}^k(t-R/c)}{R^k}, \quad k = 1, \ldots, n. \tag{39}$$

Since $R/r < 1$, the higher powers $(R/r)^k$ in (38) become vanishingly small with increasing k. This observation will be crucial in reducing both the computational effort and the storage required by the nonreflecting boundary condition – see Section 4.1. By introducing (39) into (33) and using (34), we find that the vector-valued functions $\boldsymbol{\psi}_{nm} := \{\psi_{nm}^k\}_{k=1}^n$ satisfy a system of *ordinary differential equations:*

$$\frac{1}{c}\boldsymbol{\psi}_{nm}'(t) = \frac{1}{R}\underline{\boldsymbol{A}}_n\boldsymbol{\psi}_{nm}(t) + \frac{n(n+1)}{2}U_{nm}(R,t)\boldsymbol{e}_n, \quad t > 0, \tag{40}$$

$$\boldsymbol{\psi}_{nm}(0) = \mathbf{0}. \tag{41}$$

Here the matrices $\underline{\boldsymbol{A}}_n$ are given by

$$(\underline{\boldsymbol{A}}_n)_{ij} = \begin{cases} -n(n+1)/2, & i = 1, \\ (n+i)(n-i+1)/(2i), & i = j+1, \\ 0, & \text{otherwise} \end{cases} \tag{42}$$

and the vectors $\boldsymbol{e}_n$ by

$$(\boldsymbol{e}_n)_i = \delta_{i1}, \tag{43}$$

for $i, j = 1, \ldots, n$.

The Fourier coefficients U_{nm} in (40) are computed by integration of U over the sphere $r = R$:

$$U_{nm}(R,t) = \int_0^{2\pi}\int_0^{\pi} U(R,\phi,\theta,t)\overline{Y_{nm}(\phi,\theta)}\sin\theta\,\mathrm{d}\theta\,\mathrm{d}\phi. \tag{44}$$

The Fourier expansion (35), together with (38), (40), and (44) can now be used to evaluate U in the exterior and for all time, given the boundary values of U at B [17]:

$$rU(r,\phi,\theta,t) = \sum_{n=0}^{\infty}\sum_{m=-n}^{n}(R[U_{nm}(R,\cdot)] - \sum_{k=1}^{n}\left(1-\left(\frac{R}{r}\right)^k\right)[\psi_{nm}^k])Y_{nm}(\phi,\theta), \tag{45}$$

for $r \geqslant R$. Although the functions $\boldsymbol{\psi}_{nm}$ are unknown a priori, they can be computed concurrently with U by solving (40). Thus (45) yields an explicit analytical representation of U everywhere outside B in terms of (past) values of U at B and of the auxiliary functions $\boldsymbol{\psi}_{nm}$. In contrast to the Kirchhoff formula (16), space and time are no longer coupled through an integral. Instead, for any point x in D, past values of $U_{nm}(R,\cdot)$ and $\boldsymbol{\psi}_{nm}$ are needed only from a single instant in time, which is determined by the distance of x from B. This feature will be instrumental in the derivation below.

From (36) an explicit formula for the operator M in (22) now immediately follows. Since the operator $(c^{-1}\partial_t + \partial_r)$ annihilates the first term in (36), we find that

$$\left(\frac{1}{c}\frac{\partial}{\partial t} + \frac{\partial}{\partial r}\right)(rU_{nm})(r,t) = -\frac{1}{r}\sum_{k=1}^{n} k\frac{f_{nm}^k(t-r/c)}{r^k}. \tag{46}$$

By evaluating (46) at $r = R$ and using (39), we then obtain

$$\left(\frac{1}{c}\frac{\partial}{\partial t} + \frac{\partial}{\partial r}\right)(rU_{nm})(R,t) = -\frac{1}{R}\boldsymbol{d}_n\cdot\boldsymbol{\psi}_{nm}(t), \tag{47}$$

with $\boldsymbol{d}_n = (1, 2, \ldots, n)^{\mathrm{T}}$. Multiplication of (47) with Y_{nm} and summation over n and m finally leads to an explicit formula for the operator M:

$$(MU)(\phi,\theta,t) = -\frac{1}{R}\sum_{n=1}^{\infty}\sum_{m=-n}^{n}\boldsymbol{d}_n\cdot\boldsymbol{\psi}_{nm}(t)Y_{nm}(\phi,\theta). \tag{48}$$

This operator coincides with the right-hand side in the nonreflecting boundary condition derived by Grote and Keller [13,14]. Other partial derivatives of U can also be computed by differentiation of (38). For instance,

$$\frac{1}{c}\frac{\partial U_{nm}}{\partial t}(r,t) = \frac{1}{cr}\left(R\left[\frac{\partial U_{nm}}{\partial t}(R,\cdot)\right] - \sum_{k=1}^{n}\left(1-\left(\frac{R}{r}\right)^k\right)\left[\frac{\mathrm{d}\psi_{nm}^k}{\mathrm{d}t}\right]\right), \tag{49}$$

$$\begin{aligned}\frac{\partial U_{nm}}{\partial r}(r,t) = &-\frac{1}{r^2}\left(R[U_{nm}(R,\cdot)] - \sum_{k=1}^{n}\left(1-\left(\frac{R}{r}\right)^k\right)[\psi_{nm}^k]\right)\\ &-\frac{1}{cr}\left(R\left[\frac{\partial U_{nm}}{\partial t}(R,\cdot)\right] - \sum_{k=1}^{n}\left(1-\left(\frac{R}{r}\right)^k\right)\left[\frac{\mathrm{d}\psi_{nm}^k}{\mathrm{d}t}\right]\right) - \frac{1}{r^2}\sum_{k=1}^{n}k\left(\frac{R}{r}\right)^k[\psi_{nm}^k].\end{aligned} \tag{50}$$

From (49) and (50), together with appropriate coordinate transformations, we shall now derive explicit formulas for the transfer and propagation operators P and T defined in (23)–(26).

2.3. Efficient evaluation of P and T

Outside the sphere B_j, $j = 1, 2$, we introduce local spherical coordinates (r_j, ϕ_j, θ_j) and choose the two coordinate systems by aligning their common z-axis, and having the two planes $\phi_1 = 0$ and $\phi_2 = 0$ coincide – see Fig. 3. Let d_{12} denote the (signed) distance between the two origins; note that $d_{12} < 0$ and $d_{21} > 0$. Then, the coordinates of any point on B_1 in the (r_2, ϕ_2, θ_2) coordinate system are given by

$$r_2 = \sqrt{R_1^2 - 2R_1 d_{12}\cos\theta_1 + d_{12}^2}, \tag{51}$$

$$\phi_2 = \phi_1, \tag{52}$$

$$r_2\cos\theta_2 = R_1\cos\theta_1 - d_{12}, \quad r_2\sin\theta_2 = R_1\sin\theta_1. \tag{53}$$

The normal derivative on B_1 in (r_2, ϕ_2, θ_2)-coordinates is given by

$$\frac{\partial}{\partial r_1} = \alpha_{12}(\theta_1)\frac{\partial}{\partial r_2} + \beta_{12}(\theta_1)\frac{\partial}{\partial\theta_2} \tag{54}$$

with

$$\alpha_{12}(\theta_1) = \frac{R_1 - d_{12}\cos\theta_1}{r_2}, \quad \beta_{12}(\theta_1) = -\frac{d_{12}\sin\theta_1}{r_2^2}. \tag{55}$$

From (51)–(54) we can now derive the explicit expressions for P and T by using (35). For the transfer operator T, we obtain

$$\begin{aligned}(T_{12}U_2)(\phi_1,\theta_1,t) = &R_1\sum_{n=0}^{\infty}\sum_{m=-n}^{n}\left(\frac{1}{c}\frac{\partial}{\partial t} + \alpha_{12}(\theta_1)\frac{\partial}{\partial r_2} + \frac{1}{R_1}\right)U_{2,nm}(r_2,t)Y_{nm}(\phi_2,\theta_2)\\ &+ R_1\beta_{12}(\theta_1)\sum_{n=0}^{\infty}\sum_{m=-n}^{n}U_{2,nm}(r_2,t)\frac{\partial Y_{nm}}{\partial\theta_2}(\phi_2,\theta_2),\end{aligned} \tag{56}$$

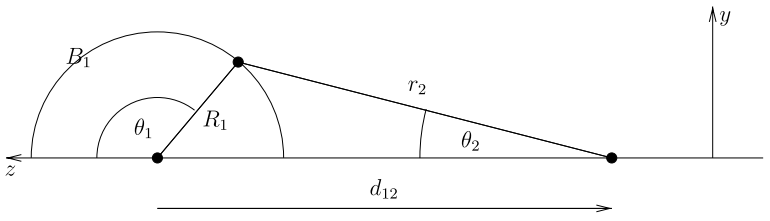

Fig. 3. Local spherical coordinates (r_1, θ_1) and (r_2, θ_2) in the yz-plane.

and for the propagation operator, P, we obtain

$$(P_{12}U_2)(\phi_1,\theta_1,t)=\sum_{n=0}^{\infty}\sum_{m=-n}^{n}U_{2,nm}(r_2,t)Y_{nm}(\phi_2,\theta_2). \tag{57}$$

The Fourier coefficients $U_{2,nm}(r_2, t)$ and its partial derivatives are evaluated by (38), (49) and (50), which involves retarded values. Explicit formulas for P_{21} and T_{21} are obtained in a similar way by exchanging the indices 1 and 2 in (56) and (57).

2.4. Well posedness

Having derived explicit formulas for the operators M, P, and T, which are needed for the nonreflecting boundary condition (18)–(21), we now state the full initial-boundary value problem for U inside the computational domain $\Omega=\Omega_1\cup\Omega_2$:

$$\frac{\partial^2 U}{\partial t^2}-\operatorname{div}(\underline{\boldsymbol{A}}\nabla U)=F \quad \text{in } \Omega\times I, \qquad I=(0,T), \tag{58}$$

$$U=U_0 \quad \text{in } \Omega\times\{0\}, \tag{59}$$

$$\frac{\partial U}{\partial t}=V_0 \quad \text{in } \Omega\times\{0\}, \tag{60}$$

$$U=G \quad \text{on } \Gamma\times I, \tag{61}$$

$$\mathscr{B}_1U:=\left(\frac{1}{c}\frac{\partial}{\partial t}+\frac{\partial}{\partial r_1}\right)(r_1U)=M_1U_1+T_{12}U_2 \quad \text{on } B_1\times I, \tag{62}$$

$$\mathscr{B}_2U:=\left(\frac{1}{c}\frac{\partial}{\partial t}+\frac{\partial}{\partial r_2}\right)(r_2U)=M_2U_2+T_{21}U_1 \quad \text{on } B_2\times I, \tag{63}$$

$$U_1+P_{12}U_2=U \quad \text{on } B_1\times I, \tag{64}$$

$$P_{21}U_1+U_2=U \quad \text{on } B_2\times I. \tag{65}$$

We shall now show that this boundary value problem has a unique solution, which coincides with the solution to the original problem (1)–(4).

Theorem 2. *Let U be the unique (strong) solution to the exterior Dirichlet problem (1)–(4) and assume that U satisfies (5)–(7) in the exterior region, $D\times I$. The two-scatterer boundary value problem (58)–(65) has a unique solution in Ω, which coincides with the restriction of U to Ω.*

Proof. *Existence*. We shall show that $U|_{\Omega\times I}$ is a solution to (58)–(65). Since U satisfies (1)–(4), it trivially satisfies (58)–(61). To show that $U|_{\Omega\times I}$ satisfies the nonreflecting boundary condition (62)–(65) on $B\times I$, we consider in $\overline{D}\times I$ the unique decomposition $U\equiv U_1+U_2$ provided by Proposition 1. Since U_1+U_2 satisfies by construction the nonreflecting boundary condition (62)–(65) on $B\times I$, so does the restriction of U to $\Omega\times I$. Therefore, $U|_{\Omega\times I}$ is a solution of the boundary value problem (58)–(65).

Uniqueness. We shall show that U can be extended from Ω into D as a C^2 solution. Then, by uniqueness of the solution in $\Omega_\infty\times I$, U will also be unique in $\Omega\times I$. Let $\widetilde{U}$ be the unique solution of the exterior boundary value problem

$$\widetilde{U}=U \quad \text{in } \Omega\times I, \tag{66}$$

$$\widetilde{U}=0,\partial_t\widetilde{U}=0 \quad \text{in } D\times\{0\}, \tag{67}$$

$$\widetilde{U}=U \quad \text{on } B\times I, \tag{68}$$

$$c^{-2}\partial_{tt}\widetilde{U}-\Delta\widetilde{U}=0 \quad \text{in } D\times I. \tag{69}$$

Because $\widetilde{U}$ is continuous on $B\times I$, all time and tangential derivatives of $\widetilde{U}$ are also continuous there. It remains to show that its normal derivative is also continuous across B. With Proposition 1 applied to $\widetilde{U}$, we obtain $\widetilde{U}=\widetilde{U}_1+\widetilde{U}_2$ in $D\times I$, where $\widetilde{U_j}=U_j$ in $D_j\times I$, $j=1,2$. From (62) and (63), we infer that $\mathscr{B}_j\widetilde{U}=$

$\mathscr{B}_j U$ on $B_j \times I$, and thus, by continuity of time and tangential derivatives of $\widetilde{U}$, we have $\partial_{r_j} \widetilde{U} = \partial_{r_j} U$ on $B_j \times I$, $j = 1, 2$. Therefore, the normal derivative of $\widetilde{U}$, together with all its time and tangential derivatives, is continuous across B, which implies that $\widetilde{U}$ is a genuine C^2 solution of the initial-boundary value problem in $\Omega_\infty \times I$. Hence, it is unique and so is its restriction U to $\Omega \times I$. □

3. Multiple scattering

The derivation of the nonreflecting boundary condition presented in Section 2 for two scatterers is easily generalized to the case of several scatterers. We consider a situation with J scatterers, and surround each scatterer by a sphere B_j of radius R_j, $j = 1, \ldots, J$. Again, we denote by $B = \bigcup_{j=1}^J B_j$ the entire artificial boundary and by D_j the unbounded region outside the jth sphere. Hence the computational domain $\Omega = \bigcup_{j=1}^J \Omega_j$, where Ω_j denotes the finite computational region inside B_j, whereas $D = \bigcap_{j=1}^J D_j$ denotes the unbounded exterior region.

In D, we now split the scattered wave into J purely outgoing waves $U_1, \ldots, U_J$, which solve the problems

$$\frac{1}{c^2}\frac{\partial^2 U_j}{\partial t^2} - \Delta U_j = 0 \quad \text{in } D_j \times I, \tag{70}$$

$$U_j = 0 \quad \text{in } D_j \times \{0\}, \tag{71}$$

$$\frac{\partial U_j}{\partial t} = 0 \quad \text{in } D_j \times \{0\} \tag{72}$$

for $j = 1, \ldots, J$. Thus, every U_j is entirely determined by its values on $B_j \times I$; it is given by (45). The matching condition is now given by

$$\sum_{j=1}^J U_j = U \quad \text{on } B. \tag{73}$$

In analogy to Proposition 1, one can show that

$$U \equiv \sum_{j=1}^J U_j \quad \text{in } \overline{D} \times I \tag{74}$$

and that this decomposition is unique. Therefore, we immediately find the nonreflecting boundary condition for a multiple scattering problem with J scatterers:

$$\mathscr{B}_j U := \left(\frac{1}{c}\frac{\partial}{\partial t} + \frac{\partial}{\partial r_j}\right)(r_j U) = M_j U_j + \sum_{\substack{\ell=1 \\ \ell \neq j}}^J T_{j\ell} U_\ell \quad \text{on } B_j \times I, \tag{75}$$

$$U_j + \sum_{\substack{\ell=1 \\ \ell \neq j}}^J P_{j\ell} U_\ell = U \quad \text{on } B_j \times I, \tag{76}$$

for $j = 1, \ldots, J$. Here M, T, and P are defined as follows:

$$M_j : U_j|_{B_j} \mapsto \mathscr{B}_j U_j|_{B_j}, \quad T_{j\ell} : U_\ell|_{B_\ell} \mapsto \mathscr{B}_j U_\ell|_{B_j}, \quad P_{j\ell} : U_\ell|_{B_\ell} \mapsto U_\ell|_{B_j}. \tag{77}$$

No additional analytical derivation due to coordinate transformation, etc. is needed once the situation of two scatterers has been resolved. Hence, M_j is given by

$$(M_j U_j)(\phi_j, \theta_j, t) = -\frac{1}{R_j}\sum_{n=1}^\infty \sum_{m=-n}^n \boldsymbol{d}_n \cdot \boldsymbol{\psi}_{j,nm}(t) Y_{nm}(\phi_j, \theta_j), \tag{78}$$

while the operators T and P are again given by (56) and (57), with '1' replaced by 'j' and '2' replaced by 'ℓ', or vice versa. Each $\boldsymbol{\psi}_{j,nm}$ solves (40) and (41), where the coefficients U_{nm} of U at B are replaced by those of U_j at B_j. For $J = 1$, (75) and (76) reduce to the nonreflecting boundary condition for a single computational domain [13,14], whereas for $J = 2$ they correspond to (62)–(65).

To further simplify the notation, we now define the (symbolic) vectors

$$\mathscr{B}U|_B = (\mathscr{B}_1 U|_{B_1}, \mathscr{B}_2 U|_{B_2}, \ldots, \mathscr{B}_J U|_{B_J})^{\mathrm{T}}, \tag{79}$$

$$U|_B = (U|_{B_1}, U|_{B_2}, \ldots, U|_{B_J})^{\mathrm{T}}, \tag{80}$$

$$U_{\mathrm{out}} = (U_1|_{B_1}, U_2|_{B_2}, \ldots, U_J|_{B_J})^{\mathrm{T}} \tag{81}$$

and the operator matrices

$$\boldsymbol{T} = \{T_{j\ell}\}_{j,\ell=1}^{J}, \quad \boldsymbol{P} = \{P_{j\ell}\}_{j,\ell=1}^{J}. \tag{82}$$

With these notations the full initial-boundary value problem in $\Omega = \cup\Omega_j$ with the nonreflecting boundary condition (75) and (76) becomes

$$\frac{\partial^2 U}{\partial t^2} - \mathrm{div}(\underline{\boldsymbol{A}}\nabla U) = F \quad \text{in } \Omega \times I, \qquad I = (0, T), \tag{83}$$

$$U = U_0 \quad \text{in } \Omega \times \{0\}, \tag{84}$$

$$\frac{\partial U}{\partial t} = V_0 \quad \text{in } \Omega \times \{0\}, \tag{85}$$

$$U = G \quad \text{on } \Gamma \times I, \tag{86}$$

$$\mathscr{B}U = \boldsymbol{T}U_{\mathrm{out}} \quad \text{on } B \times I, \tag{87}$$

$$\boldsymbol{P}U_{\mathrm{out}} = U \quad \text{on } B \times I. \tag{88}$$

4. Efficient implementation and discretization

We consider the multiple scattering problem (83)–(88) and let N_h be the typical number of grid points in Ω_j in any space dimension. Hence the work per time step, W_Ω, for any standard finite difference or finite element method in the interior will be proportional to N_h^3, and so will be the storage required, S_Ω. We shall now show how to efficiently evaluate the terms appearing in (87) and (88) so that the additional computational work, W_B, and storage, S_B, due to the nonreflecting boundary condition, scale like N_h^3 as well. Then, we shall discuss in detail a typical implementation of (83)–(88) and exhibit the full algorithm.

4.1. Work and storage

In practice, the series (45) used in the nonreflecting boundary condition (87) and (88) is truncated at some finite number, N_B. We let U_{N_B} denote the corresponding approximation,

$$U_{N_B}(r,\phi,\theta,t) := \frac{R}{r}\sum_{n=0}^{N_B}\sum_{m=-n}^{n}[U_{nm}(R,\cdot)]Y_{nm}(\phi,\theta) + -\frac{1}{r}\sum_{n=1}^{N_B}\sum_{m=-n}^{n}\sum_{k=1}^{n}\left(1-\left(\frac{R}{r}\right)^k\right)[\psi_{nm}^k]Y_{nm}(\phi,\theta). \tag{89}$$

The truncation error $\|U - U_{N_B}\|_2$ is bounded from above by $N_B^{-(k+1)}$ if $U \in C^k$, due to spectral accuracy. Because the discretization error in the interior typically decays no faster than N_h^{-p} for any pth order discretization, the two errors are comparable for N_B typically much smaller than N_h (for reasonably smooth solutions).

To reduce the amount of work due to the propagation and transfer operators, we shall further approximate (89) by neglecting vanishingly small terms in the triple sum. For $K_B \leqslant N_B$, we thus define

$$\begin{aligned} U_{N_B,K_B}(r,\phi,\theta,t) := {} & \frac{R}{r}\sum_{n=0}^{N_B}\sum_{m=-n}^{n}[U_{nm}(R,\cdot)]Y_{nm}(\phi,\theta) + -\frac{1}{r}\sum_{n=1}^{N_B}\sum_{m=-n}^{n}\left[\sum_{k=1}^{n}\psi_{nm}^k\right]Y_{nm}(\phi,\theta) \\ & + \frac{1}{r}\sum_{n=1}^{N_B}\sum_{m=-n}^{n}\sum_{k=1}^{\min\{n,K_B\}}\left(\frac{R}{r}\right)^k\left[\psi_{nm}^k\right]Y_{nm}(\phi,\theta). \end{aligned} \tag{90}$$

Recall that the square brackets denote time retarded values. The error due to this second approximation behaves like $(R/r)^{-(K_B+2)}$. Since R/r is strictly smaller than 1, that error decays exponentially fast; therefore, we can choose K_B much smaller than N_B, independently of the mesh size.

Next, we define

$$\psi^{\Sigma}_{nm}(t) := \sum_{k=1}^{n} \psi^{k}_{nm}(t). \tag{91}$$

For each (n, m) we need to store the value of ψ^{Σ}_{nm} and the individual values of ψ^{k}_{nm}, but only for $k = 1, \ldots, \min\{n, K_B\}$. As a consequence, the storage required for the ψ^{k}_{nm} in (90) is reduced from $O(N_B^3)$ to $O(N_B^2 K_B)$.

Evaluation of M. To efficiently evaluate MU we rewrite (48) as

$$(MU)(\phi,\theta,t) = -\frac{1}{R}\sum_{m=-N_B}^{N_B} \underbrace{\sum_{n=\max\{|m|,1\}}^{N_B} \boldsymbol{d}_n \cdot \boldsymbol{\psi}_{nm}(t)\, c_{nm} P_n^{|m|}(\cos\theta)}\, \mathrm{e}^{\mathrm{i}m\phi}. \tag{92}$$

Here, we first evaluate the inner bracket (for each n, m), then the outer bracket (for each m, θ), and finally the whole expression (for each ϕ, θ), which requires $O(N_B^3)$, $O(N_B^2 N_h)$, and $O(N_B N_h^2)$ operations, respectively.

To compute $\boldsymbol{\psi}_{nm}(t)$ we need to solve the differential equations (40). If we opt for implicit time stepping, an $n \times n$ linear system needs to be solved at each time step for every (n, m), $n \leqslant N_B$. Clearly, the LU decomposition of the matrices $\underline{\boldsymbol{I}} - c\Delta t(2R)^{-1}\underline{\boldsymbol{A}}_n$ (see also Section 4.2) then needs to be computed only once. Hence, the work per time step scales at worst like N_B^4, because of the forward and backward substitutions for the solution the systems of linear equations, $n = 1, \ldots, N_B$, $|m| \leqslant n$, each of size $n \times n$ – see (109). Usually N_B^4 is negligible because N_B is small, yet for large values it can be reduced to N_B^3 by using either compression techniques [1,25,28], or predictor–corrector time integrators since $\underline{\boldsymbol{A}}_n$ is sparse. The storage required for the solution of (40) and (41) also scales like N_B^3, because the matrices $\underline{\boldsymbol{A}}_n$ only depend on n.

In (40) the integral

$$U_{nm}(R,t) = c_{nm} \int_0^{\pi} \underbrace{\int_0^{2\pi} U(R,\phi,\theta,t)\mathrm{e}^{-\mathrm{i}m\phi}\,\mathrm{d}\phi}\, P_n^{|m|}(\cos\theta)\sin\theta\,\mathrm{d}\theta, \tag{93}$$

is first evaluated over ϕ, for every $m = -N_B, \ldots, N_B$ and for all grid values of θ, which requires $O(N_B N_h^2)$ operations. Then, the remaining *one-dimensional* integrals over θ are evaluated for all n and m, which requires $O(N_B^2 N_h)$ operations. The computational cost for the evaluation of the Fourier coefficients U_{nm} may be further reduced with a fast transformation method [27].

Evaluation of P. The operator $P_{j\ell}$ applied to U_ℓ is evaluated on B_j as

$$(P_{j\ell}U_\ell)(\phi_j,\theta_j,t) = \sum_{m=-N_{B_\ell}}^{N_{B_\ell}} \underbrace{\sum_{n=|m|}^{N_{B_\ell}} U_{\ell,nm}(r_\ell,t)\, c_{nm} P_n^{|m|}(\cos\theta_\ell)}\, \mathrm{e}^{\mathrm{i}m\phi_\ell}. \tag{94}$$

Because $\phi_\ell = \phi_j$, the distance $r_\ell(\theta_j)$ from the center of B_ℓ to $(R_j, \theta_j) \in B_j$ depends only on θ_j. Indeed, the relation between the j- and ℓ-coordinates on the artificial boundary component B_j is given by

$$r_\ell \sin\theta_\ell = R_j \sin\theta_j, \tag{95}$$

$$r_\ell \cos\theta_\ell = R_j \cos\theta_j - d_{j\ell}. \tag{96}$$

As a consequence of this key observation, the outer bracket in (94) is independent of ϕ_j and hence needs to be computed only for every n, m, and θ_j. Each Fourier coefficient $U_{\ell,nm}$ in (90) is evaluated by

$$r_\ell U_{\ell,nm}(r_\ell,t) \simeq R_\ell[U_{\ell,nm}(R_\ell,\cdot)] - [\psi^{\Sigma}_{\ell,nm}] + \sum_{k=1}^{\min\{n,K_{B_\ell}\}} \left(\frac{R_\ell}{r_\ell}\right)^k [\psi^{k}_{\ell,nm}], \tag{97}$$

again after truncation at K_{B_ℓ}. The accuracy of the approximation (97) has been analyzed in [17]. The work involved in (94) is $O(N_{B_\ell}^2 K_{B_\ell} N_h)$, $O(N_{B_\ell}^2 N_h)$, and $O(N_{B_\ell} N_h^2)$ operations, respectively.

When three or more subdomains are present, the z-axes must be aligned pairwise. Then the propagated field $P_{j\ell}U_\ell$ must be interpolated at grid points in the (fixed) local coordinate system on B_j. The additional cost for

this interpolation also scales like N_h^2 and is therefore included in the work estimate above. The computational cost can be further reduced by tabulating and storing the values of the spherical harmonics in advance, at the required grid points.

Evaluation of T. The operator $T_{j\ell}$ applied to U_ℓ and evaluated on B_j is given by

$$(T_{j\ell}U_\ell)(\phi_j,\theta_j,t) = R_j \sum_{n=0}^{N_{B_\ell}} \sum_{m=-n}^{n} \left(\frac{1}{c}\frac{\partial}{\partial t} + \alpha_{j\ell}(\theta_j)\frac{\partial}{\partial r_\ell} + \frac{1}{R_j}\right) U_{\ell,nm}(r_\ell,t) Y_{nm}(\phi_\ell,\theta_\ell) + R_j \beta_{j\ell}(\theta_j) \sum_{n=0}^{N_{B_\ell}} \sum_{m=-n}^{n} U_{\ell,nm}(r_\ell,t) \frac{\partial Y_{nm}}{\partial \theta_\ell}(\phi_\ell,\theta_\ell), \tag{98}$$

where the Fourier coefficients are again approximated by (97). By definition of the retarded values for a time-dependent function f, we have

$$[f] = [f](r_\ell,t) = f\left(t - \frac{r_\ell - R_\ell}{c}\right), \tag{99}$$

$$\frac{1}{c}\frac{\partial [f]}{\partial t} = -\frac{\partial [f]}{\partial r_\ell} = \frac{1}{c}[f']. \tag{100}$$

The partial derivatives of $U_{\ell,nm}$ are obtained via finite differences applied to the retarded time derivatives of $U_{\ell,nm}(R_\ell,\cdot)$, $\psi^k_{\ell,nm}$ and $\psi^\Sigma_{\ell,nm}$. Hence, the work requirements are of the same order as for the propagation operator, namely $O(N_{B_\ell}^2 K_{B_\ell} N_h + N_{B_\ell} N_h^2)$ operations.

Storage of past values. The storage of the retarded values of $U_{\ell,nm}(R_\ell,\cdot)$, $\psi^k_{\ell,nm}$, and $\psi^\Sigma_{\ell,nm}$ is essentially given by $O(m_\ell N_{B_\ell}^2)$, $O(m_\ell N_{B_\ell}^2 K_{B_\ell})$, and $O(m_\ell N_{B_\ell}^2)$, respectively. Here m_ℓ denotes the number of time steps any wave needs to propagate from B_ℓ to the farthest point on any other sphere B_j, $j \neq \ell$. It is given by

$$m_\ell = \left\lceil \frac{\max_{j\neq\ell}(d_{\ell j} + R_j) - R_\ell}{c\Delta t} \right\rceil, \quad \ell = 1,\ldots,J, \tag{101}$$

and hence depends linearly on the problem size. Due to Huygens' principle *only a finite time window of the past needs to be stored*, whose size depends only on the geometry of the problem; in particular, it is independent of the final time of the computation.

Total cost and storage. Gathering the above work and storage estimates we find that the work and storage required for the nonreflecting boundary condition (87) and (88) at B_ℓ scale like

$$W_{B_\ell} = O(N_{B_\ell} N_h^2 + N_{B_\ell}^2 K_{B_\ell} N_h + N_{B_\ell}^3), \tag{102}$$

$$S_{B_\ell} = O(m_\ell N_{B_\ell}^2 K_{B_\ell} + N_{B_\ell}^3), \quad \ell = 1,\ldots,J. \tag{103}$$

Here we assume that any one of the techniques mentioned earlier in this section has been used to reduce the cost for the solution of the systems of ordinary differential equations from N_B^4 to N_B^3. With $N_t := \max_{\ell\in\{1,\ldots,J\}} m_\ell$ (the maximal number of retarded values to be stored on any boundary component), $N_B := \max_{\ell\in\{1,\ldots,J\}} N_{B_\ell}$, and $K_B := \max_{\ell\in\{1,\ldots,J\}} K_{B_\ell}$, the total work and storage for the nonreflecting boundary condition (87) and (88) scales like

$$W_B = O(N_B N_h^2 + K_B N_B^2 N_h + N_B^3), \tag{104}$$

$$S_B = O(K_B N_t N_B^2 + N_B^3). \tag{105}$$

Because K_B is independent of the mesh size, and hence independent of N_h, while N_B scales at worst like N_h, we have shown that the amount of total work per time step due to the nonreflecting boundary condition scales at worst like $O(N_h^3)$, which corresponds to the computational effort of the numerical scheme inside Ω. The storage of past values, which cannot be avoided, is kept minimal by storing Fourier coefficients instead of grid values and by judiciously employing the rapid decay of higher modes $n > K_B$ with increasing distance from their respective subdomains.

4.2. Finite difference discretization

We shall now show how to discretize the nonreflecting boundary condition in (83)–(88) with a standard second-order finite difference scheme. In each sub-domain Ω_j, we choose local spherical coordinates and an equidistant grid along the artificial boundary, for simplicity. We denote by N_r the corresponding radial index of the grid points located at a typical B_j. The time interval $I=(0,T)$ is discretized at equidistant points $t_k = k\Delta t$, $k = 0, 1, \ldots$

Next, we denote by U_i^k the values of the numerical solution at $r = r_i$ and at time t_k, and discretize (83) by second-order central finite differences in space and time. Omitting the sub-domain index j, a finite difference discretization of (83) at $i = N_r$ reduces to

$$0 = \frac{U_{N_r}^{k+1} - 2U_{N_r}^k + U_{N_r}^{k-1}}{c^2\Delta t^2} - \frac{1}{R^2}(\Delta_S^h U)_{N_r}^k - \frac{\left(R+\frac{\Delta r}{2}\right)^2 U_{N_r+1}^k - 2\left(R^2+\frac{\Delta r^2}{4}\right)U_{N_r}^k + \left(R-\frac{\Delta r}{2}\right)^2 U_{N_r-1}^k}{R^2\Delta r^2} \tag{106}$$

with Δ_S^h a finite difference approximation of the Laplace–Beltrami operator (29).

The values on the "ghost layer" $i = N_r + 1$, which appear in (106), are eliminated via second-order discretization of the boundary condition (87) and of the matching condition (88),

$$R\frac{U_{N_r}^{k+1} - U_{N_r}^{k-1}}{2c\Delta t} + \frac{(R+\Delta r)U_{N_r+1}^k - (R-\Delta r)U_{N_r-1}^k}{2\Delta r} = (\boldsymbol{T}U_{\text{out}})^k, \tag{107}$$

$$(\boldsymbol{P}U_{\text{out}})^k = U_{N_r}^k. \tag{108}$$

Here, $R = R_j$ denotes the radius of the artificial boundary B_j, U_{out} denotes the auxiliary values on all boundary components (81), $(\boldsymbol{T}U_{\text{out}})^k$ denotes the values on the right-hand side of (87) at time t_k, $(\boldsymbol{P}U_{\text{out}})^k$ denotes the values on the left-hand side of (88) at time t_k, and $c > 0$ denotes the wave speed. The ordinary differential equations (40) are discretized for instance with the unconditionally stable implicit trapezoidal rule

$$\left(\underline{\boldsymbol{I}} - \frac{c\Delta t}{2R}\underline{\boldsymbol{A}}_n\right)\boldsymbol{\psi}_{nm}^k = \left(\underline{\boldsymbol{I}} + \frac{c\Delta t}{2R}\underline{\boldsymbol{A}}_n\right)\boldsymbol{\psi}_{nm}^{k-1} + \frac{c\Delta t}{2}\frac{n(n+1)}{2}(U_{nm}^k + U_{nm}^{k-1})\boldsymbol{e}_n. \tag{109}$$

Thus, we finally obtain the following numerical scheme for the solution of (88), (84)–(88).

Algorithm

- Initialize U^0 and U^1 in $\overline{\Omega}$.
- Initialize the Fourier coefficients of U_{out}^0 and $\boldsymbol{\psi}_{nm}^0$.
- At each time step t_k, given U^k, U^{k-1}, and past values of U_{out}, $\boldsymbol{\psi}_{nm}$:
  - compute U_{out}^k by (76), using (94) and (97);
  - compute the Fourier coefficients of U_{out}^k by (93);
  - advance $\boldsymbol{\psi}_{nm}^k$ using (109);
  - advance U^{k+1} inside Ω;
  - compute $(\boldsymbol{T}U_{\text{out}})^k$ from (98) and (97);
  - compute $U_{N_r}^{k+1}$ by (106) and (107).

Except for the numerical solution of the small ordinary differential equation system in (40), the algorithm above is fully explicit in time. Moreover, both the computations inside individual subdomains Ω_j and those at their respective artificial boundaries B_j can be computed independently of each other, and in parallel.

5. Numerical results

To assess the accuracy of the nonreflecting boundary condition for multiple scattering (87) and (88) we shall now combine it with a finite difference method, as described in Section 4, and apply it to a series of test problems. First, we shall consider a simple model problem, for which the exact solution is known. It is just to compute the radiating wave field of a transient point source in a homogeneous medium, as it propagates

through the two disjoint components of our computational domain, Ω. Second, we shall present computations for scattering from two sound-soft spheres; in particular, we shall compare the numerical solution obtained from a true multiple scattering approach with that obtained by embedding the two obstacles in a single much larger domain. Third, we shall compute the scattered field from a transient plane wave packet impinging on two spheres. All three test problems are axisymmetric about the z-axis, so that the solution U is independent of ϕ.

5.1. Accuracy and convergence study

To verify the accuracy and convergence of the numerical method, we first consider the following simple test problem, where U corresponds to an outgoing spherical wave that originates from an off-centered point source at $\boldsymbol{c}_2 + (0, d)$ on the z-axis – see Fig. 4. The wave profile $g = g(x)$ is chosen twice continuously differentiable and such that $U = 0$ in the exterior at $t = 0$. The exact values of U are prescribed on the boundaries Γ_1 and Γ_2 of the two "obstacles", located at $r_1 = a_1$ and $r_2 = a_2$, respectively. Hence, the exact solution in (r_2, θ_2)-coordinates is given by

$$U(r_2, \theta_2, t) = \frac{g(r' - ct)}{r'}, \qquad r' = \left\| \begin{pmatrix} r_2 \sin\theta_2 \\ r_2 \cos\theta_2 \end{pmatrix} - \begin{pmatrix} 0 \\ d \end{pmatrix} \right\|, \quad t \geqslant 0 \tag{110}$$

with $0 \leqslant d < a_2$. We choose $\boldsymbol{c}_1 = (0, 1)$, $\boldsymbol{c}_2 = (0, -1)$, $a_1 = 0.5$, $a_2 = 0.6$, $R_1 = 1$, $R_2 = 0.9$, and $d = 0.4$ – see Fig. 4. Note that the singularity at $r' = 0$ is of no concern here, because that point lies strictly outside Ω.

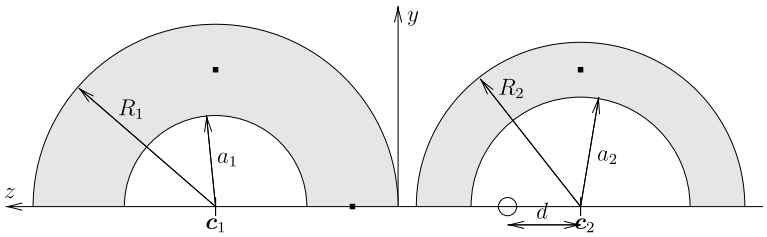

Fig. 4. The geometry used for the numerical examples. The shaded region is the computational domain Ω.

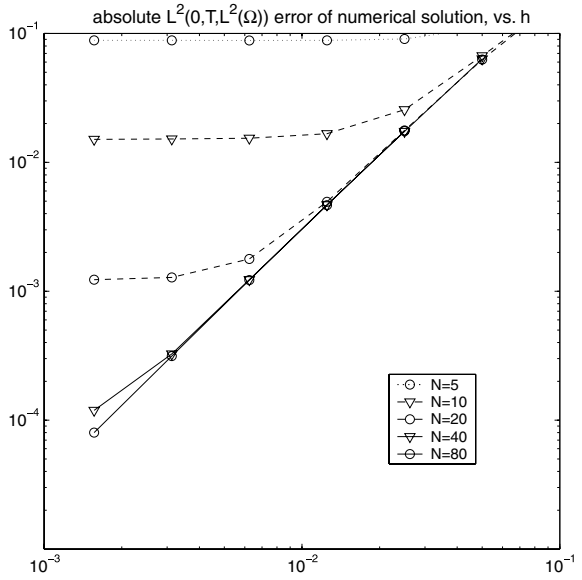

Fig. 5. The total L^2-error is shown vs. the mesh size h for different values of N_B.

Since the boundary condition (87) and (88) on the artificial boundaries at $r_j = R_j$, $j = 1, 2$, is exact, the numerical solution in Ω must converge to the exact solution inside Ω, as the mesh size $h \to 0$ and the time step $\Delta t \to 0$. To verify this fact, we compute the solution until $T = 8$, while monitoring the L^2-error with respect to the exact solution,

$$E^h(t) := \|U_{\text{ex}}(\cdot,\cdot,t) - U_{\text{num}}(\cdot,\cdot,t)\|_{L^2(\Omega)}$$

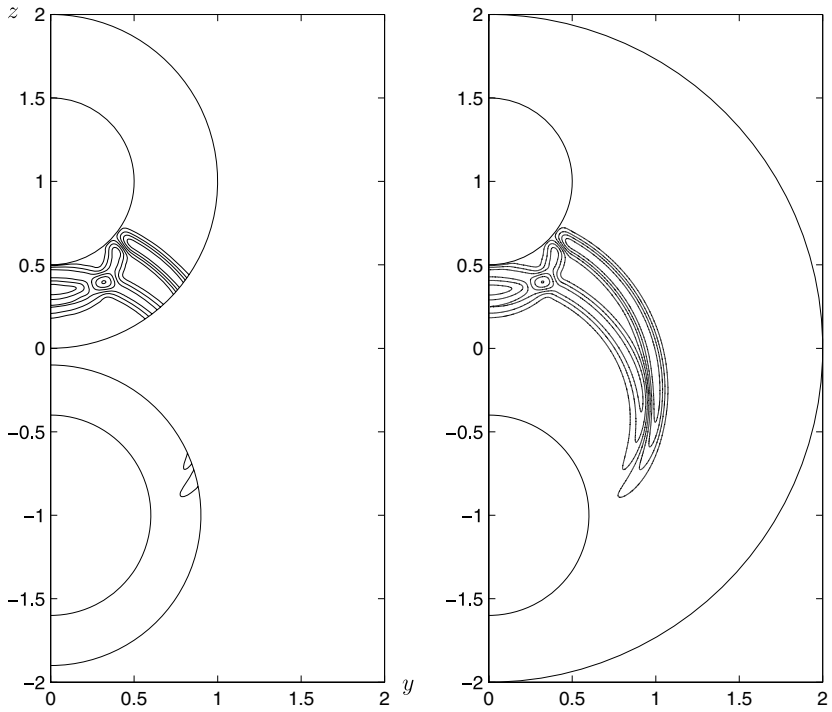

Fig. 6. Scattering from two sound-soft spheres. Contour lines of the wave field are shown at time $t = 1$. (Left) The numerical solution obtained by a second-order finite difference method combined with the nonreflecting boundary condition for multiple scattering (87) and (88); (right) the numerical solution obtained by a finite element method combined with the nonreflecting boundary condition for a single computational domain (48).

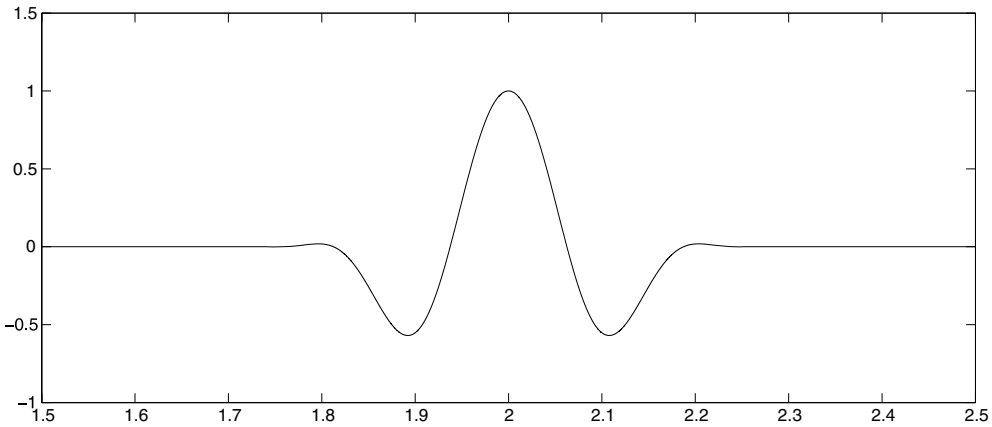

Fig. 7. Plane wave scattering: the profile of the wave packet is shown.

at each time step. In Fig. 5, the total L^2-error $\|E^h(t)\|_{L^2(0,T)}$ is shown vs. h for different truncation indices N_B (see Section 4). For $N_B = 80$, we observe global second-order convergence of the method for the entire mesh sequence considered here. Here, and in all subsequent computations we use $K_B = 50$ in (97) because the obstacles are rather close to each other.

In Fig. 5, we also observe the subtle interplay between the approximation error in the boundary condition, controlled by N_B, and that due to discretization in the interior of Ω. For small values of N_B, the error due to truncation tends to dominate, so that further mesh refinement does not improve the accuracy. In contrast, if we keep the mesh fixed at $h \simeq 0.01$, for instance, we observe no further improvement in accuracy from increasing N_B up to 80; in fact, with $N_B = 20$ the level of accuracy imposed by the discretization inside Ω has already been reached. In general convergence can only be achieved by systematically reducing h while increasing N_B, simultaneously.

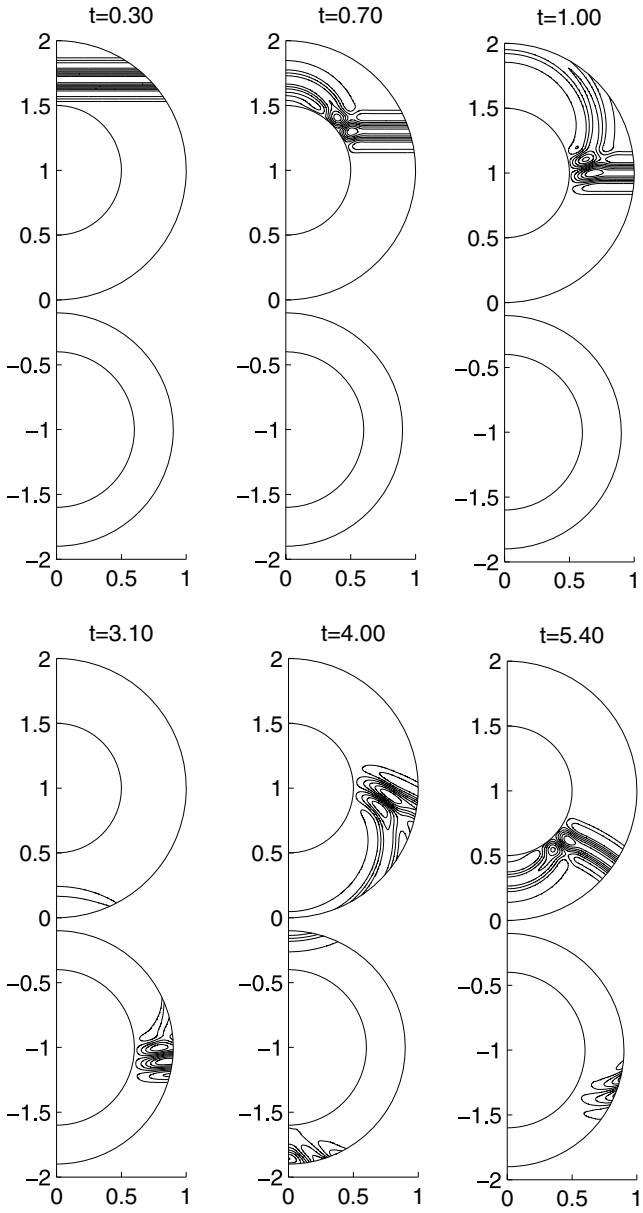

Fig. 8. Plane wave scattering: the total wave field is shown at selected instants in time.

5.2. Comparison with the solution in a single computational domain

Next, we consider acoustic scattering from two sound-soft spheres located at $\boldsymbol{c}_1$, $\boldsymbol{c}_2$ and with radii a_1, a_2, respectively – see Fig. 4; hence, U vanishes on the boundaries of the two obstacles. Here we choose the same parameter values as in the previous test problem. At $t = 0$, we set both U and $\partial_t U$ to zero throughout Ω, but for a small region about $(y, z) = (0, -0.25)$. There, a smooth initial disturbance in the velocity field generates an outgoing wave, which impinges on the second and later on the first obstacle above. Then, the propagating

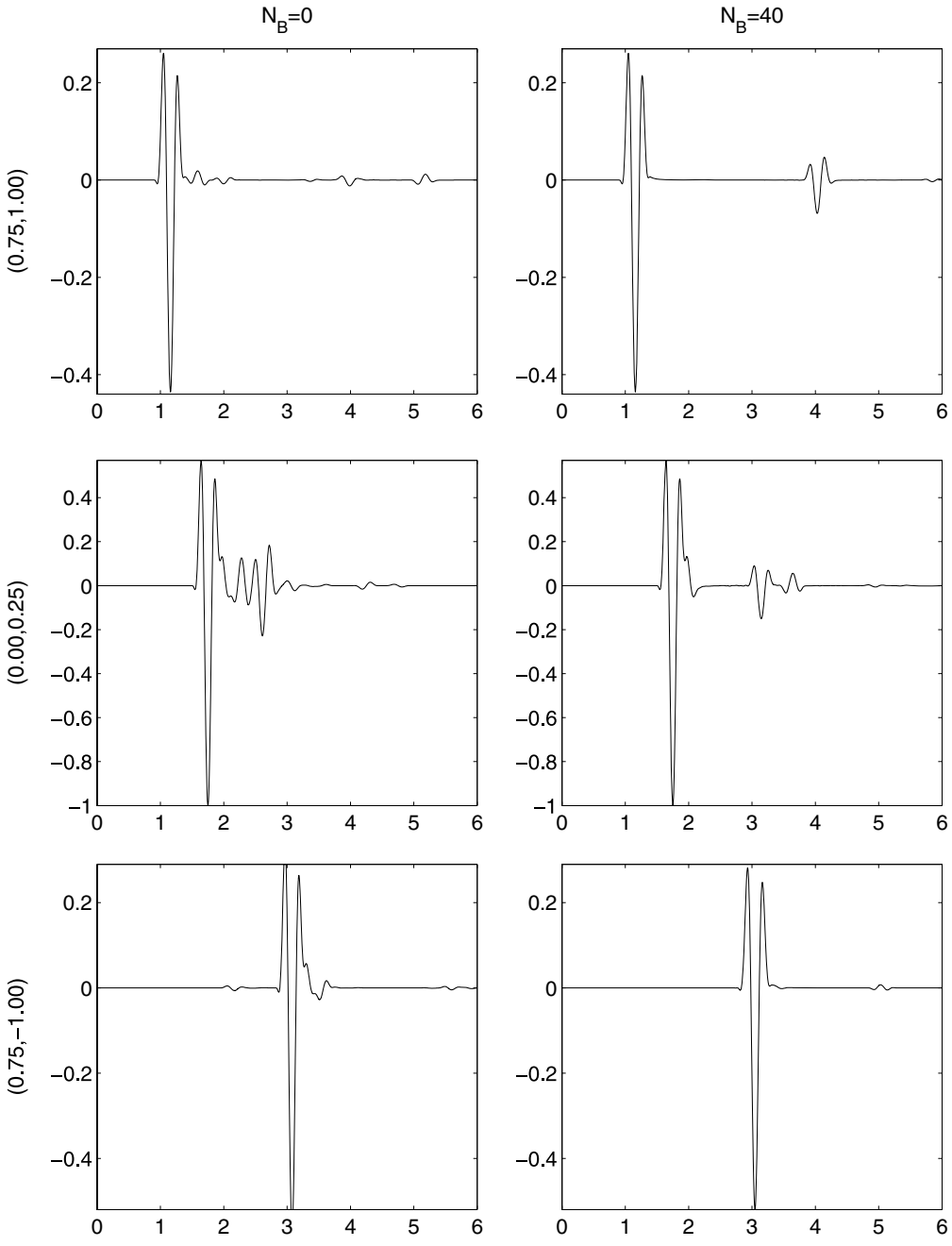

Fig. 9. Plane wave scattering: the total wave at three selected points in space over time – see Fig. 4 – for $N_B = 0$ and $N_B = 40$.

wave circumvents the upper sphere, while multiple reflections occur between the two obstacles, repeatedly shedding waves as they move back and forth.

To verify the accuracy of the boundary condition for multiple scattering (87) and (88) we now compare the numerical solution obtained by using a finite difference scheme, with that obtained in a single larger computational domain that contains the two obstacles; here, the nonreflecting boundary condition (48) is imposed at the artificial spherical boundary $R = 2$ – see [14] for a finite element formulation. As shown in Fig. 6, the two numerical solutions, displayed at time $t = 1$, coincide inside Ω.

5.3. Plane wave scattering

Finally, we consider an incident plane wave packet $U^i(\boldsymbol{x}, t) = f(z + t)$ impinging upon two sound-soft spheres; its profile is shown in Fig. 7. The scattered field, U^s, thus satisfies $U^s = -U^i$ on the surface of the two obstacles.

In Fig. 8, the numerical solution with the nonreflecting boundary condition for multiple scattering (87) and (88) is shown at selected instants in time. At time $t = 0$ the incident plane wave penetrates Ω_1 from above and impinges upon the upper sphere. Then, the incident plane wave proceeds downward until it leaves Ω_1 at time $t \simeq 2$. It later reaches Ω_2 and is reflected by the lower obstacle. The scattered wave propagates upward back into Ω_1, where again it is reflected by the upper obstacle. By $t \simeq 4$, the incident wave packet has entirely left Ω, yet the scattered waves remain; they bounce back and forth between the two obstacles while continuously radiating energy into the surrounding unbounded medium.

In Fig. 9 we illustrate the influence of truncation at N_B on the accuracy of the nonreflecting boundary condition. To do so, we compare two numerical solutions, obtained either with $N_B = 40$ or $N_B = 0$, at three selected points in space – see Fig. 4. We remark that setting $N_B = 0$ in (87) and (88) corresponds to approximating the decomposition of U in the two purely outgoing wave fields U_1, U_2 outside Ω by two spherically symmetric wave fields, $U = U_1(r_1, t) + U_2(r_2, t)$. In that case the boundary operator $\mathscr{B}$ reduces to the first-order Bayliss–Turkel condition [3] while the extension operators $\boldsymbol{P}$ and $\boldsymbol{T}$ essentially approximate the incoming part arriving from the other obstacle by spherical waves; thus, the effect of the other obstacle is (crudely) replaced by that of a simple point source.

The two upper frames show the time evolution of the solution at a point on the east of the upper sphere. That location is first reached by the incident plane wave, and again at later time by the first reflection from the lower obstacle. With $N_B = 0$, this second arrival is barely visible, accompanied by various spurious signals. In Fig. 9, the two middle frames show the solution below the south pole of the upper obstacle. For $N_B = 0$, spurious reflection occurs from the artificial boundary B_1, which obscures the reflected wave propagating upwards. Moreover, the plane wave is propagated into Ω_2 with rather poor accuracy. For $N_B = 40$, however, the plane wave passes the artificial boundaries B_1, B_2 without spurious reflections, before it impinges upon the lower obstacle; then, the reflected wave again crosses B_2 and B_1 to re-enter Ω_1. This behavior is correctly reproduced with $N_B = 40$, but rather poorly with $N_B = 0$.

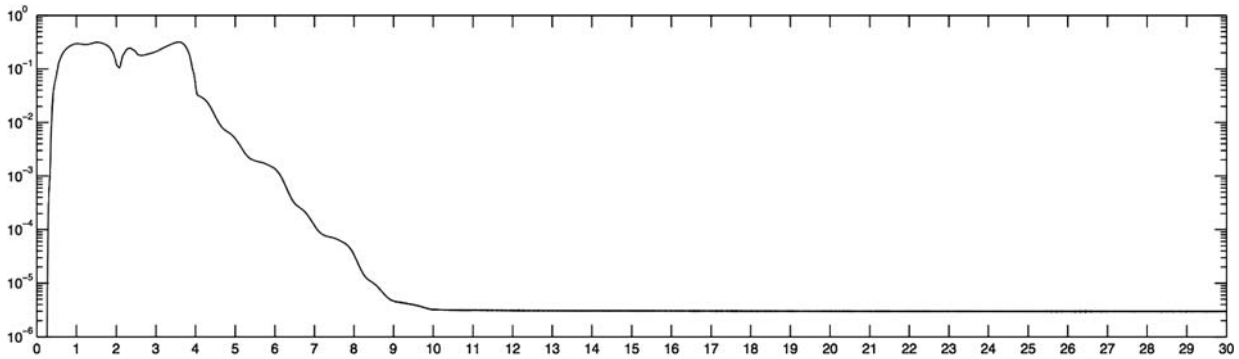

Fig. 10. Plane wave scattering: the L_2-norm of the numerical solution ($N_B = K_B = 50$) is shown vs. time to illustrate the overall stability of our numerical scheme.

The two lower frames in Fig. 9 show the solution at a point on the east of the lower obstacle. The incident wave first reaches this point, followed by the reflection from the upper obstacle. For $N_B = 0$, the incident plane wave is distorted by spurious reflection while the arrival time of the reflected wave is incorrect. Furthermore, for $N_B = 0$, a spurious signal *precedes* the incident wave packet, due the over-simplified representation of U in the exterior. With $N_B = 40$, sufficiently many Fourier modes are included in the nonreflecting boundary condition to accurately represent the exterior wave field: no spurious precursor appears in that case.

Finally, to verify the numerical stability of the scheme over a long time, we show in Fig. 10 the approximate L_2-norm of the numerical solution in Ω vs. time.

6. Conclusion

We have derived an exact nonreflecting boundary condition (NBC) for time-dependent multiple scattering problems in three space dimensions, which holds when the artificial boundary B consists of a union of disjoint spherical components. It is given by (87) and (88) and avoids spurious reflection from B. We have proved that the NBC for multiple scattering leads to a well-posed initial-boundary value problem in the computational domain Ω, and that its solution coincides with the restriction to Ω of the solution in the infinite region.

The NBC involves only first-order derivatives; therefore, it is easily coupled with finite difference or finite element methods. Hence, the full numerical scheme retains the global rate of convergence of the interior scheme, while the computational work due to the NBC only involves a fraction of the computational work inside Ω, independently of the mesh size or the desired overall accuracy. Both high accuracy and convergence of the method have been demonstrated via numerical experiments with a standard second-order finite difference method.

Because the artificial boundary no longer needs to be convex, the size of the computational domain can be chosen much smaller than with standard absorbing boundary conditions or perfectly matched layers; moreover, the size of the computational domain no longer increases with the relative distances between the various sub-scatterers. Although the artificial boundary must be of simple geometric shape, here a union of disjoint spheres, the NBC is not tied to any particular coordinate system.

The derivation of the NBC for multiple scattering is based on the decomposition of the scattered field in several purely outgoing wave fields. A similar approach was previously used by the authors to derive a Dirichlet-to-Neumann boundary condition for *time-harmonic* multiple scattering [18]. The same approach can be used to derive exact NBCs for multiple scattering for other wave equations or geometries, such as ellipsoids or wave guides, for which the NBC with a single (convex) artificial boundary is explicitly known. In particular, the derivation presented here extends to time-dependent electromagnetic and elastic wave scattering, where similar boundary conditions are known [11,15,16].

The computational work required by the NBC for multiple scattering asymptotically scales like the work required by any standard finite difference or finite element method in the interior and, in practice, it is only a fraction of it. The storage of past values is kept minimal by storing Fourier coefficients instead of grid values and by judiciously employing the rapid decay of certain components of higher Fourier modes with increasing distance from their respective subdomains. At the expense of a more complicated implementation, further reduction in the work and storage could probably be attained by employing advanced compression techniques in time [1,25] for the past of the auxiliary functions $\psi_{nm}(t)$ needed in the NBC, or a fast transform for spherical harmonics [27].

References

[1] B. Alpert, L. Greengard, T. Hagstrom, Rapid evaluation of nonreflecting boundary kernels for time-domain wave propagation, SIAM J. Numer. Anal. 37 (4) (2000) 1138–1164.
[2] B.B. Baker, E.T. Copson, The Mathematical Theory of Huygens' Principle, Oxford University Press, Oxford, 1939.
[3] A. Bayliss, E. Turkel, Radiation boundary conditions for wave-like equations, Comm. Pure Appl. Math. 33 (6) (1980) 707–725.
[4] E. Bécache, S. Fauqueux, P. Joly, Stability of perfectly matched layers, group velocities and anisotropic waves, J. Comput. Phys. 188 (2) (2003) 399–433.
[5] J.-P. Bérenger, A perfectly matched layer for the absorption of electromagnetic waves, J. Comput. Phys. 114 (2) (1994) 185–200.

[6] Q.Y. Chen, T. Tang, Z.-H. Teng, A fast numerical method for integral equations of the first kind with logarithmic kernel using mesh grading, J. Comput. Math. 22 (2) (2004) 287–298.
[7] F. Collino, P. Monk, The perfectly matched layer in curvilinear coordinates, SIAM J. Sci. Comput. 19 (6) (1998) 2061–2090.
[8] B. Engquist, A. Majda, Absorbing boundary conditions for the numerical simulation of waves, Math. Comput. 31 (139) (1977) 629–651.
[9] A.A. Ergin, B. Shanker, E. Michielssen, Fast evaluation of three-dimensional transient wave fields using diagonal translation operators, J. Comput. Phys. 146 (1) (1998) 157–180.
[10] D. Givoli, D. Cohen, Nonreflecting boundary conditions based on Kirchhoff-type formulae, J. Comput. Phys. 117 (1) (1995) 102–113.
[11] M.J. Grote, Nonreflecting boundary conditions for elastodynamic scattering, J. Comput. Phys. 161 (1) (2000) 331–353.
[12] M.J. Grote, Local nonreflecting boundary condition for Maxwell's equations, Comput. Methods Appl. Mech. Eng. 195 (2006) 3691–3708.
[13] M.J. Grote, J.B. Keller, Exact nonreflecting boundary conditions for the time dependent wave equation, SIAM J. Appl. Math. 55 (2) (1995) 280–297.
[14] M.J. Grote, J.B. Keller, Nonreflecting boundary conditions for time-dependent scattering, J. Comput. Phys. 127 (1) (1996) 52–65.
[15] M.J. Grote, J.B. Keller, Nonreflecting boundary conditions for Maxwell's equations, J. Comput. Phys. 139 (2) (1998) 327–342.
[16] M.J. Grote, J.B. Keller, Exact nonreflecting boundary conditions for elastic waves, SIAM J. Appl. Math. 60 (3) (2000) 803–819.
[17] M.J. Grote, C. Kirsch, Far-field evaluation via nonreflecting boundary conditions, in: T.Y. Hou, E. Tadmor (Eds.), Hyperbolic Problems: Theory, Numerics, Applications, Springer, Berlin, 2003, pp. 195–204.
[18] M.J. Grote, C. Kirsch, Dirichlet-to-Neumann boundary conditions for multiple scattering problems, J. Comput. Phys. 201 (2) (2004) 630–650.
[19] T. Ha-Duong, B. Ludwig, I. Terrasse, A Galerkin BEM for transient acoustic scattering by an absorbing obstacle, Int. J. Numer. Methods Eng. 57 (13) (2003) 1845–1882.
[20] T. Hagstrom, Radiation boundary conditions for the numerical simulation of waves, Acta Numer. 8 (1999) 47–106.
[21] T. Hagstrom, S.I. Hariharan, A formulation of asymptotic and exact boundary conditions using local operators, Appl. Numer. Math. 27 (4) (1998) 403–416.
[22] T. Hagstrom, T. Warburton, A new auxiliary variable formulation of high-order local radiation boundary conditions: corner compatibility conditions and extensions to first-order systems, Wave Motion 39 (4) (2004) 327–338.
[23] E.W. Hobson, The Theory of Spherical and Ellipsoidal Harmonics, Cambridge University Press, Cambridge, 1931.
[24] A.E.H. Love, Wave-motions with discontinuities at wave-fronts, Proc. London Math. Soc. II 1 (1904) 37–62.
[25] C. Lubich, A. Schädle, Fast convolution for nonreflecting boundary conditions, SIAM J. Sci. Comput. 24 (1) (2002) 161–182.
[26] P.A. Martin, Multiple scattering: an invitation, in: G. Cohen (Ed.), Mathematical and Numerical Aspects of Wave Propagation, SIAM, 1995, pp. 3–16.
[27] M.J. Mohlenkamp, A fast transform for spherical harmonics, J. Fourier Anal. Appl. 5 (1999) 159–184.
[28] I.L. Sofronov, Artificial boundary conditions of absolute transparency for two- and three-dimensional external time-dependent scattering problems, Eur. J. Appl. Math. 9 (6) (1998) 561–588.
[29] Z.-H. Teng, Exact boundary condition for time-dependent wave equation based on boundary integral, J. Comput. Phys. 190 (2) (2003) 398–418.
[30] L. Ting, M.J. Miksis, Exact boundary conditions for scattering problems, J. Acoust. Soc. Am. 80 (6) (1986) 1825–1827.
[31] S.V. Tsynkov, Numerical solution of problems on unbounded domains. A review, Appl. Numer. Math. 27 (4) (1998) 465–532.
[32] C.H. Wilcox, A generalization of theorems of Rellich and Atkinson, Proc. Am. Math. Soc. 7 (1956) 271–276.